Biosensors and Bioelectronics 190 (2021) 113371

Contents lists available at ScienceDirect

Biosensors and Bioelectronics

journal homepage: www.elsevier.com/locate/bios

$Ru(bpy)_3^{2+}$ encapsulated cyclodextrin based metal organic framework with improved biocompatibility for sensitive electrochemiluminescence detection of CYFRA21-1 in cell

Yunfei Wang, Yixiao Li, Xuming Zhuang *, Chunyuan Tian, Xiuli Fu, Feng Luan **

College of Chemistry and Chemical Engineering, Yantai University, Yantai, 264005, China

ARTICLE INFO

Keywords:
Electrochemiluminescence biosensor
Cyclodextrin
Metal organic framework
CYFRA21-1
Biomarker
Lung cancer

ABSTRACT

Metal-organic frameworks (MOFs) have attracted strong interest from researchers. Here, for the first time, we report a sandwich-type electrochemiluminescent biosensor as a signal probe prepared from cyclodextrin-based MOF (CD-MOF)-encapsulated $Ru(bpy)_3^{2+}$. Due to the combination of the two materials, the obtained CD-MOF@$Ru(bpy)_3^{2+}$ nanocomposites exhibited excellent biocompatibility and electrochemical performance. At the same time, CD-MOF@$Ru(bpy)_3^{2+}$ adhered to the electrode surface closely because $Ru(bpy)_3^{2+}$ was successfully encapsulated by the CD-MOF. In this paper, CD-MOF@$Ru(bpy)_3^{2+}$ and glutaraldehyde were modified on a glassy carbon electrode (GCE) surface to provide excellent conductivity and to immobilize primary antibodies. Under the optimal experimental conditions, the established biosensor exhibited high sensitivity, a low limit of detection and a great linear range for cytokeratin 19 fragment antigen 21-1 (CYFRA21-1). Finally, this designed biosensor was further applied to the determination of CYFRA21-1 in A549 lung cancer cells. According to the results of the toxicity test, CD-MOF@$Ru(bpy)_3^{2+}$ exhibited hypotoxicity to living bodies. These results all indicate that this biosensor has great potential for a promising approach to the evaluation of biomarkers.

1. Introduction

According to statistics, tens of millions of new cancer cases emerged every year, and half of them end in cancer death [Bray et al., 2018]. Therefore, cancer has proven to be the deadliest disease in the world to date. Among the different kinds of cancers, lung cancer is the leading cause of cancer deaths worldwide [Aizer et al., 2015; Torre et al., 2015; Waki et al., 2014]. In general, lung cancer can be divided into two main subtypes: small cell lung cancer (SCLC) and non-small-cell lung cancer (NSCLC) [Han et al., 2008; Yang et al., 2019]. It has been reported that the NSCLC type accounts for approximately 80–85% of total lung cancer cases [Chen et al., 2015]. Therefore, it is important diagnosis NSCLC in a timely manner, which could be helpful in improving the survival rate of patients. It has been proven that the level of tumour markers in the serum of some cancer patients is relevant to the severity of the cancer [Fang et al., 2019; Zeng et al., 2018]. Thus, the accurate determination of tumour markers has attracted worldwide attention in the search for early diagnosis [Fang et al., 2019; Zeng et al., 2018]. For this, the cytokeratin 19 fragment (CYFRA21-1), a 36 kDa fragment of cytokeratin 19 located in the cytoskeleton of epithelial cells, has been considered an effective tumour marker for the detection of lung cancer, and especially for the diagnosis of NSCLC [Ferrigno et al., 2003]. Various methods have been reported for the detection of CYFRA21-1, including electrochemical immunoassay [Zhu et al., 2015], electrochemical DNA biosensing [Chen et al., 2018], electrochemical immunoassay [Yu et al., 2016], electrochemiluminescence (ECL) [Xu et al., 2015], etc. Among these methods, ECL has received considerable attention due to its simple instrumentation, easy miniaturization and high sensitivity.

With the development of ECL methods, an increase number of luminous materials have been found and applied to ECL analysis in recent years [Li et al., 2009]. $Ru(bpy)_3^{2+}$ is one of the materials with particular promise due to its high solubility in water, high stability and long excited state life. In addition, $Ru(bpy)_3^{2+}$ is sensitive and quick to use for ECL detection, and no additional light source or spectroscopic system is required for the analysis, which greatly improves the reproducibility of the experiment [Li et al., 2009; Miao et al., 2008, Richter, 2004]. This material has been widely used in the determination of persulfate [White and Bard et al., 1982], alkylamines [Lee and Nieman, 1995], organic

* Corresponding author.
** Corresponding author.
E-mail addresses: xmzhuang@iccas.ac.cn (X. Zhuang), fluan@sina.com (F. Luan).

https://doi.org/10.1016/j.bios.2021.113371
Received 16 February 2021; Received in revised form 16 May 2021; Accepted 19 May 2021
Available online 30 May 2021

acids [Rubinstein and Bard et al., 1981] and so on. In addition, according to the results reported by Rubinstein and Bard, $Ru(bpy)_3^{2+}$ can be regenerated at the electrode surface during an ECL reaction [Rubinstein and Bard et al., 1981]. Therefore, it maybe significant to develop an effective method to immobilize $Ru(bpy)_3^{2+}$ on the electrode surface. However, there are some drawbacks of $Ru(bpy)_3^{2+}$, such as low stability, which encourages researchers to introduce other materials to improve performance.

Metal organic frameworks (MOFs), which are made up of organic ligands and metal ions, are yet another kind of new material [Hua et al., 2014]. They have attracted increasing attention from researchers and have been favour in the last few years because of their large specific surface areas, permanent porosities, and high electron transfer rates on the electrode surface [Peng et al., 2020; Trino et al., 2021]. In recent years, MOFs have been applied in storage, catalysis, electrochemical and so on, and they also have potential applications as biosensors and in other fields [Al-Kutubi et al., 2015]. However, the shortcoming of MOFs is that they often exhibit poor biocompatibility. On this basis, cyclodextrin (CD) was introduced into a MOF to synthesize CD-MOF, which had exhibited great biocompatibility, and CD as a kind of edible natural products, it could build the cubic CD-MOF by combining with K^+ under the suitable temperature and pressure. Besides, the MOF for excellent electrochemical performance was used to encapsulate $Ru(bpy)_3^{2+}$ successfully and build an ECL sensor, and the obtained sensor had the synergistic amplification effect of the CD-MOF and $Ru(bpy)_3^{2+}$ and could further make up the shortcomings of the $Ru(bpy)_3^{2+}$ which mentioned above.

Herein, a sandwich-type ECL sensor was developed in this study which is based on CD-MOF encapsulated $Ru(bpy)_3^{2+}$ (CD-MOF@Ru$(bpy)_3^{2+}$) by the hydrothermal method, and further used it to determine CYFRA 21-1, the principle was shown in Scheme 1. In this paper, the electron transfer process of $Ru(bpy)_3^{2+}$ was facilitated and the stability of the sensor was improved [Huang et al., 2008; Li et al., 2009]. Furthermore, to connect the CD-MOF@$Ru(bpy)_3^{2+}$ nanocomposites to the antibody protein, the common bifunctional crosslinking agent glutaraldehyde (GA) was used. Moreover, 0.1 M Tris-HCl containing tripropylamine (TPA) was used as the co-reactant, and CdTe nanoparticles (NPs) were used in this project as quenching agents to scavenge ECL energy from the CD-MOF@$Ru(bpy)_3^{2+}$ electrode. Finally, the proposed ECL biosensor was successfully used for the determination of CYFRA21-1 in serum and A549 lung cancer cells, and the results showed that this sensor was capable for clinical assays and exhibited great promise in the future.

2. Experimental

2.1. Reagents and apparatus

Beta-cyclodextrin (β-CD), potassium hydroxide (KOH), absolute ethanol (C_2H_5OH), Nafion, acetone (CH_3COCH_3), $C_{30}H_{24}Cl_2N_6Ru_6H_2O$ $(Rubpy)_3Cl_2$, glutaraldehyde (GA), chromium dichloride ($CdCl_2$), sodium borohydride ($NaBH_4$) and TPA were obtained from Sinopharm Chemical Reagent Co. Ltd. (Beijing China). Bovine serum albumin (BSA), 3-(4,5dimethylthiazolyl)-2,5 dimethylthiazol-2-yl)-2,5 diphenyltetrazolium bromide (MTT), 3-mercaptopropionic acid (MPA), dimethyl sulfoxide (DMSO), ascorbic acid (AA), and uric acid (UA) were obtained from Sigma-Aldrich (St. Louis, MO, USA). Cytokeratin 19 fragment antigen21-1 (CYFRA21-1) and cytokeratin 19 fragment antigen21-1 antibodies (antiCYFRA21-1) were purchased from Linc-Bio Science Co. (Shanghai, China). Prostate protein antigen (PSA), carcinoembryonic antigen (CEA) and fetoprotein (AFP) were purchased from the Huayang Zhenglong Biochemical Lab (Chengdu, China). Nanopure deionized and distilled water (DDW) (18.2 MΩ cm^{-1}) was used throughout the experiments.

The ECL measurements were performed on a CHI660B electrochemical workstation (Chenhua Instruments, Shanghai, China). The microstructure and morphology of the samples were characterized by transmission electron microscopy (TEM, JEOL-2010F, 200 kV) and elemental mapping (APOLLOX). X-ray diffraction (XRD, LabX XRD-6000) was used to characterize the crystallinity of the obtained nanomaterials. The cells were cultured in a humidified incubator (Thermo Scientific 3111). X-ray photoelectron spectroscopy (XPS) was conducted on a Thermo ESCALAB 250 (USA). A conventional three-electrode system was used to carry out all electrochemical measurements, that is glassy carbon electrode (GCE), platinum wire, and Ag/AgCl (in 3 M KCl) as the working, auxiliary, and reference electrodes, respectively. All experiments were performed room temperature.

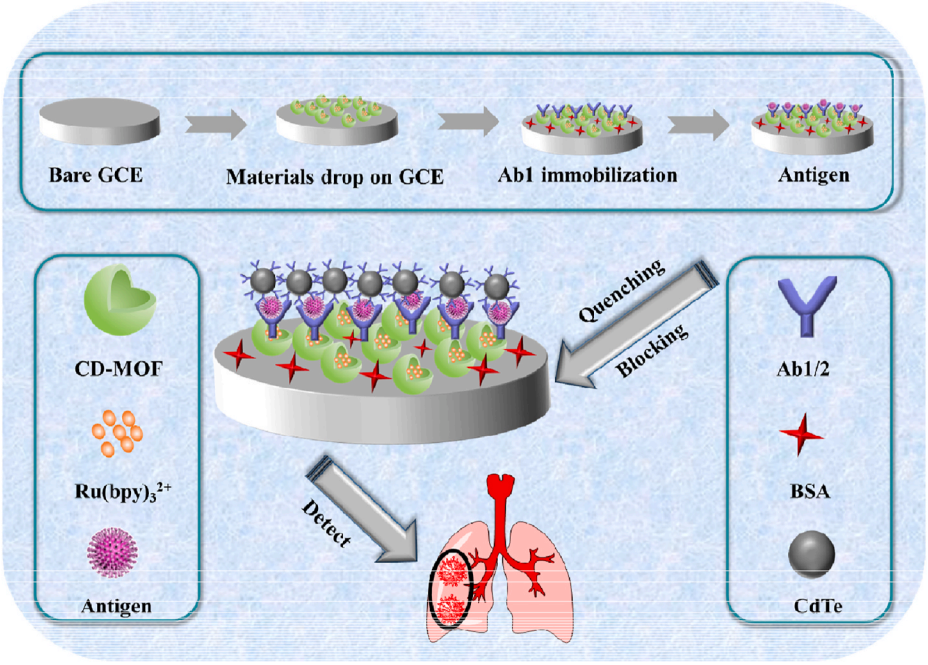

Scheme 1. Schematic of the synthesis of the CD-MOF@$Ru(bpy)_3^{2+}$ nanocomposites for detecting CYFRA21-1.

2.2. Preparation of CD-MOF and CD-MOF@Ru(bpy)$_3^{2+}$

CD-MOF was obtained following the procedure reported in the previously previous [Moussa et al., 2016]. On this basis, CD-MOF@Ru(bpy)$_3^{2+}$ was synthesized as follows. Briefly, 1.2 g β-CD, 0.5 g KOH, and 2 mg Ru(bpy)$_3^{2+}$ were dissolved in 15 mL DDW/ethanol (4:6) solution under magnetic stirring for 30 min. Then, the solution of the mixture was transferred to a reactor, and the reactor was placed in an electric blast air drying box for 3 day at 100 °C. The resulting substance was centrifuged three times in the DDW/ethanol (4:6) solution and dried in air to obtain CD-MOF@Ru(bpy)$_3^{2+}$. The CD-MOF was prepared and treated under the same experimental conditions but without adding Ru(bpy)$_3^{2+}$.

2.3. Synthesized of the CdTe NPs

The CdTe NPs were synthesized according to reference [Tian et al., 2012]. At first, $CdCl_2$•$2.5H_2O$ was dissolved in ultrapure water, then MPA was added and N_2 was used to deaerate the solution. After then, tellurium powder and $NaBH_4$ were dissolved in water at 60 °C under vigorous stirring to prepare an oxygen-free NaHTe solution. Following, the NaHTe solution was added to the mixture solution (described above), and the new solution was refluxed at 100 °C for approximately 3 h to get CdTe NPs.

Then, the obtained CdTe NPs were treated to activate the carboxyl groups on the surface according to the following steps. At first, 1.0 mg CdTe NPs was dispersed in 1-methylimidazol aqueous solution (0.1 M, pH = 7.4) containing 25 mg mL^{-1} EDC and 12 mg mL^{-1} NHS. Subsequently, the mixed solution was left at room temperature for 1.5 h. After activation, CdTe NPs were separated by centrifugation and alternately washed with water and PBS three times. And then, the mixture was redissolved in 1.0 mL PBS (0.1 M, pH = 7.4). The activated CdTe NPs were obtained and kept at 4 °C until use.

2.4. Fabrication of the ECL biosensor

Before nanocomposites were modified on the GCE, it was polished for approximately three or 4 min using aluminite powder. And then, the GCE was cleaned ultrasonically three times using DDW and ethyl alcohol respectively. Every GCE was tested by determining the cyclic voltammogram for a 1.0 mM $K_3Fe(CN)_6$ solution containing 0.1 M KCl and the amperometry signals were recorded at a constant potential (−0.08 V). To modify the GCE, 10 μL of the CD-MOF@Ru(bpy)$_3^{2+}$ (2 mg mL^{-1}) nanocomposites were dropped on the GCE surface and evaporated in air. After drying of the electrode, 10 μL of 0.25% Nafion was also dropped on the electrode in order to fix the Ru(bpy)$_3^{2+}$ onto the electrode effectively. The thickness of the membrane directly affects the ion-exchange capacity and electron transfer velocity. When it was dried in air at room temperature, the GCE was denoted as CD-MOF@Ru(bpy)$_3^{2+}$/GCE.

Then, the CD-MOF@Ru(bpy)$_3^{2+}$/GCE was activated with 2.5% GA for 2 h at room temperature followed by the washing with ultrapure water. Subsequently, 5 μL of 50 μg mL^{-1} Ab1 was added to the CD-MOF@Ru(bpy)$_3^{2+}$/GCE with a reaction time of 15 h and temperature of 4 °C. Then, 3% BSA was added to the electrode for approximately 1 h to block remaining active sites. After being washed with water and PBS, the prepared Ab1/GA/CD-MOF@Ru(bpy)$_3^{2+}$/GCE was incubated with different concentrations of CYFRA21-1 for 1 h at 37 °C. Finally, the cells were further incubated with 100 μL of Ab2/CdTe solution for 1 h at room temperature. In the end, the obtained biosensor was washed with 0.1 M PBS and water, and then stored at 4 °C before use for the detection of CYFRA21-1.

2.5. Cell toxicity assay

In order to test the toxicity of CD-MOF@Ru(bpy)$_3^{2+}$ to A549 cells, MTT was used to measure the absorbance. In this experiment, A549 lung carcinoma cells were cultured in a 96-well cell culture plate, at a final level of 8000 cells per well. Next, different volumes (1, 2.5, 5, 7.5, 10, 15 μL) of CD-MOF@Ru(bpy)$_3^{2+}$ (2 mg mL^{-1}) were added into wells, and then the cells were incubated at 37 °C under 5% CO_2. After approximately 24 h, MTT was added to the wells to a final concentration of 5 mg mL^{-1}, and then the cell culture plate was incubated under the same conditions for approximately 4 h. Finally, MTT formazan was dissolved in 150 μL DMSO and the absorbance at 570 nm was measured by enzyme-linked immunoassay.

3. Results and discussion

3.1. Characterizations of the nanocomposites

TEM was employed to investigate the surface morphologies of the prepared nanocomposites, as shown in Fig. 1. In the absence of Ru(bpy)$_3^{2+}$ (Fig. 1A), the CD-MOF exhibited a single uniform fold structure, and showed a uniformly dispersed morphology. It was clear that the two materials were successfully attached after they were combined (Fig. 1B), and Ru(bpy)$_3^{2+}$ was well dispersed in the CD-MOF. Therefore, this proved that the CD-MOF@Ru(bpy)$_3^{2+}$ nanocomposites were synthesized successfully. In addition, EDX analysis (Fig. S1) was also performed to confirm the presence of C, O, K, Ru and Cl in CD-MOF@Ru(bpy)$_3^{2+}$, and these elements were homogeneously distributed throughout the nanocomposites.

Furthermore, XRD was carried out to study the composition and crystal structures of the prepared CD-MOF@Ru(bpy)$_3^{2+}$ nanocomposites. As shown in Fig. S2, the characteristic diffraction peaks at 2θ = 12.7, 17.6 and 40.5° corresponded to the crystalline planes of CD-MOF nanoparticles, which was consistent with reports in the literature [Luan et al., 2020; Panella and Hirscher et al., 2010]. In addition, the XRD peaks at 2θ = 28.37, 50.29 and 58.71° corresponded to the crystalline planes of Ru(bpy)$_3^{2+}$. Altogether, the XRD spectra confirmed that Ru(bpy)$_3^{2+}$ was successfully wrapped in the CD-MOF.

XPS was performed to analyse the elemental composition and valence states of the elements in the prepared CD-MOF@Ru(bpy)$_3^{2+}$ nanocomposites. Ru, C, O, and Cl were all detected throughout the nanocomposite material. Fig. 1C clearly shows that there are six peaks at approximately 199.01, 268.59, 284.33 and 534.85 eV, which could be attributed to Cl 2p, Ru 3d, C 1s and O 1s ionizations, respectively. In addition, Fig. 1D shows that two kinds of carbon bonds were found: C–O at 289.47 eV and C–C at 286.80 eV in the C 1s spectra. These results confirmed that the CD-MOF@Ru(bpy)$_3^{2+}$ nanocomposites were synthesized successfully.

In addition, the ECL intensity of CD-MOF@Ru(bpy)$_3^{2+}$/GCE was measured from 400 nm to 680 nm under a series of optical filters, and the results are shown in Fig. S3A. The maximum ECL intensity was at approximately 600 nm. To further explore its properties, the fluorescence intensity of the nanocomposite was measured with an excitation wavelength of 365 nm. The result in Fig. S3B displays its maximum emission wavelength at 600 nm, which corresponds to the results obtained with optical filters.

To further explore the performance of CdTe NPs as quenching agents, TEM images were obtained and are shown in Fig. S4A. This shows CdTe NPs with diameters of approximately 5–10 nm. In addition, Fig. S4B shows the normalized UV–Vis spectrum of CdTe NPs; there was broad absorption in the wavelength range 300–900 nm and no exciton emission peak. These results demonstrate that CdTe NPs are a black-body-like material and can be used as an effective quencher of ECL in this experiment.

3.2. Optimizations of detection conditions

According to previous literature [Luan et al., 2020], the concentration of Ru(bpy)$_3^{2+}$ and the pH both affect the ECL performance. Therefore, the concentration of Ru(bpy)$_3^{2+}$ and pH were optimized first, and

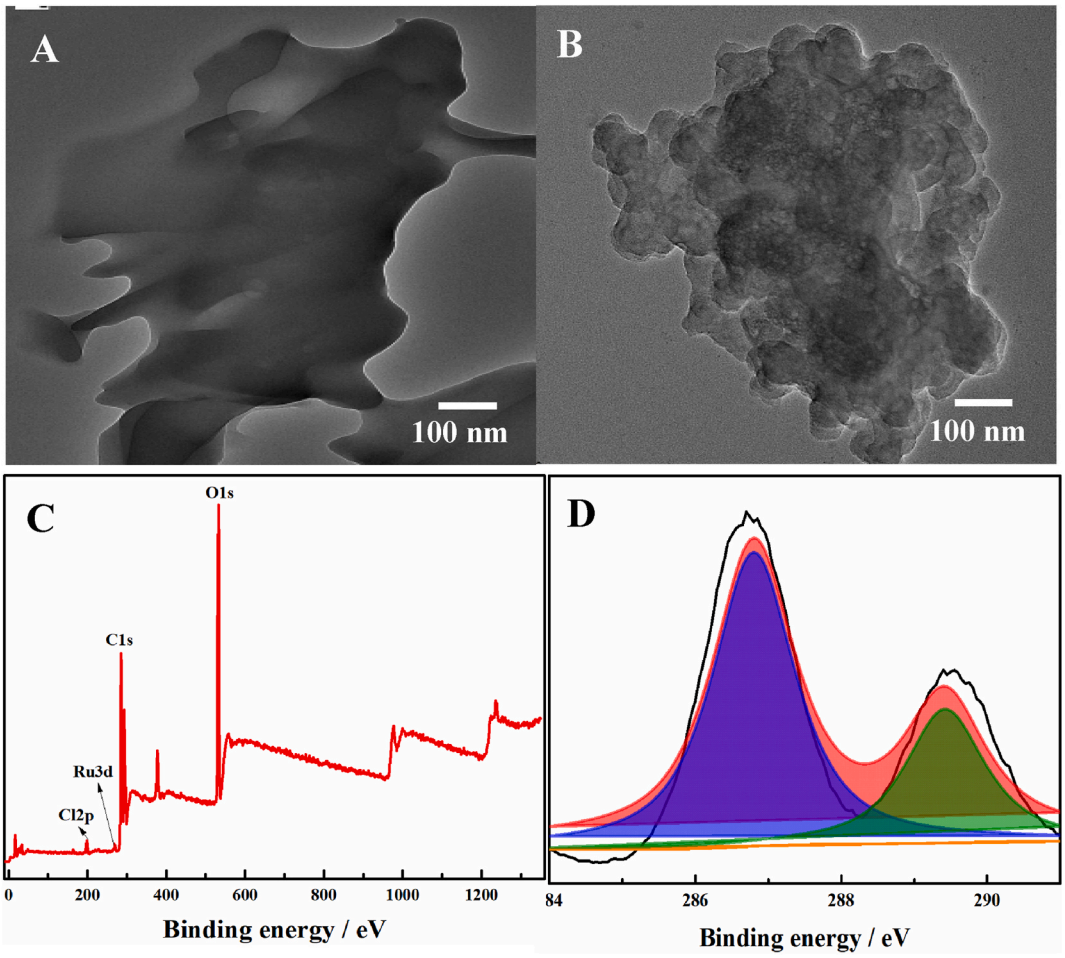

Fig. 1. TEM images of (A) CD-MOF, and (B) CD-MOF@Ru(bpy)$_3^{2+}$ nanocomposites. (C) XPS spectrum and (D) High-resolution C1s of CD-MOF@Ru(bpy)$_3^{2+}$ nanocomposites.

the results were shown in Fig. S5A. The ECL intensity exhibited the strongest signal when the concentration was 0.2 mM within the range of 0.02–1.00 mM. Thus, 0.2 mM Ru(bpy)$_3^{2+}$ was selected as the optimal concentration.

Next, the same GCE was fabricated and investigated within the pH range 3.0–13.0. Fig. S5B showed that the ECL intensity increased as the pH increased from 3.0 to 7.4 and then, decreased gradually as the pH was raised from 7.4 to 13.0. Thus, a pH 7.4 Tris-HCl (0.1 M) buffer solution was selected as the optimal environment for detection in all experiments.

3.3. ECL behaviour of CD-MOF and CD-MOF@Ru(bpy)$_3^{2+}$

The electrochemical and ECL behaviours of CD-MOF and CD-MOF@Ru(bpy)$_3^{2+}$ were investigated with 0.1 M Tris-HCl that contained TPA as the co-reactant. It was clearly seen in Fig. 2A that there was no significant ECL intensity of CD-MOF, and when Ru(bpy)$_3^{2+}$ was modified on the CD-MOF, the ECL response increased about to 60,000. According

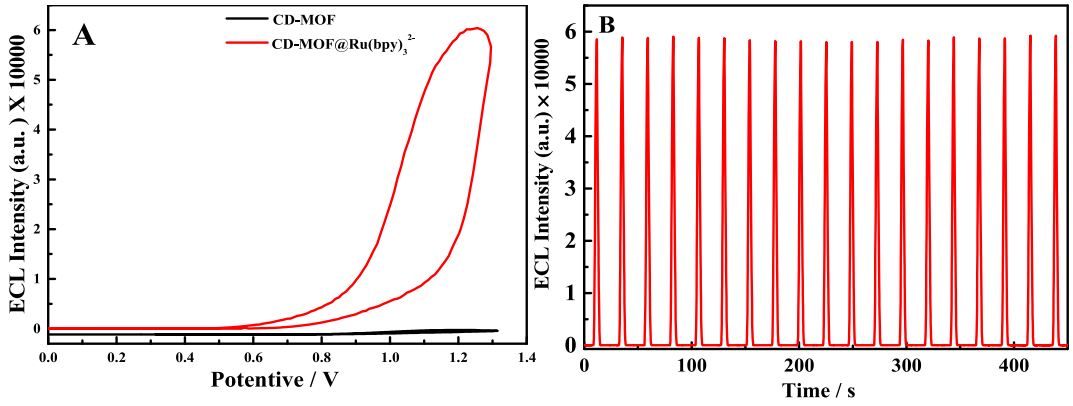

Fig. 2. (A) The ECL curves of the CD-MOF and CD-MOF@Ru(bpy)$_3^{2+}$ in 0.1M Tris-HCl containing TPA at pH 7.4 and a 600 V PMT at a scan rate of 100 mV s^{-1}. (B) ECL emission from the CD-MOF@Ru(bpy)$_3^{2+}$ under continuously cyclic scans in 0.1 M Tris-HCl with a pH of 7.4 and a 600 V PMT.

to the results reported in the previous literature [Huang et al., 2013; Jia et al., 2009; Sun et al., 2009], the mechanism for the ECL generated with CD-MOF@Ru(bpy)$_3^{2+}$ in buffer solution could be illustrated as follows:

$$Ru(bpy)_3^{2+} - e^- \rightarrow Ru(bpy)_3^{3+} \quad (1)$$

$$Ru(bpy)_3^{3+} + TPA \rightarrow TPA^{\bullet+} + Ru(bpy)_3^{2+} \quad (2)$$

$$TPA - e^- \rightarrow TPA^{\bullet+} \quad (3)$$

$$TPA^{\bullet+} - H^+ \rightarrow TPA^{\bullet} \quad (4)$$

$$Ru(bpy)_3^{3+} + TPA \rightarrow TPA+ + Ru(bpy)_3^{2+} \quad (5)$$

$$Ru(bpy)_3^{2+*} \rightarrow Ru(bpy)_3^{2+} + h\nu \quad (6)$$

In this experiment, CD-MOF@Ru(bpy)$_3^{2+}$ was chosen as the ECL-emitting material, and it produced strong ECL phenomenon in the co-reagent 0.1 M Tris-HCl (pH 7.4) containing TPA. At the same time, CdTe NPs were used to as the quenching agent and absorbed the light emitted by CD-MOF@Ru(bpy)$_3^{2+}$. Utilizing this mechanism, an ECL biosensor was built and used to detect the CYFRA21-1 cell marker.

3.4. ECL response of the biosensor to the CYFRA21-1

The obtained electrochemical biosensor was further investigated using different concentrations of the CYFRA21-1 as shown in Fig. 3. It could be found from Fig. 3A, when the Ab1 was captured on the CD-MOF@Ru(bpy)$_3^{2+}$ (blue line), the ECL intensity decrease slightly, which could be attributed to the fact that Ab1 was not conductive. After CYFRA21-1 was assembled onto the electrode (red line), the ECL intensity obviously decreased, which is because of the blockage of electron transfer by inert protein molecules. Finally, after the CD-MOF@Ru(bpy)$_3^{2+}$/Ab1/CYFRA21-1 was incubated in the solution of CdTe/Ab2 (black line), the ECL intensity was quenched by approximately 92%. This result was attributed to the immunoreaction of CYFRA21-1 with immobilized anti-CYFRA21-1, which produced a nonconductive complex that blocked electron transfer between ECL reagents and the electrode surface. Additionally, the corresponding cyclic voltammetry (CV) curves of the CD-MOF@Ru(bpy)$_3^{2+}$ nanocomposite and antibody-conjugated materials were showed in Fig. S7A. A reduction current was seen when the potential was approximately 1.2 V, which was attributed to the reduction of TPA on the electrode surface. And the different values of the currents could be due to the effects of steric hindrance between the CD-MOF@Ru(bpy)$_3^{2+}$ nanocomposite and different antibody-conjugated materials.

Fig. 3B was the ECL intensity response of CD-MOF@Ru(bpy)$_3^{2+}$ in HCl-Tris (pH = 7.4) containing TPA and different concentrations of CYFRA21-1 ranging from 0.1 to 200 ng mL^{-1}. It was showed that with the concentration of CYFRA21-1 was increased, the ECL intensity clearly decreased (Fig. 3C). However, Fig. 3D showed that when the

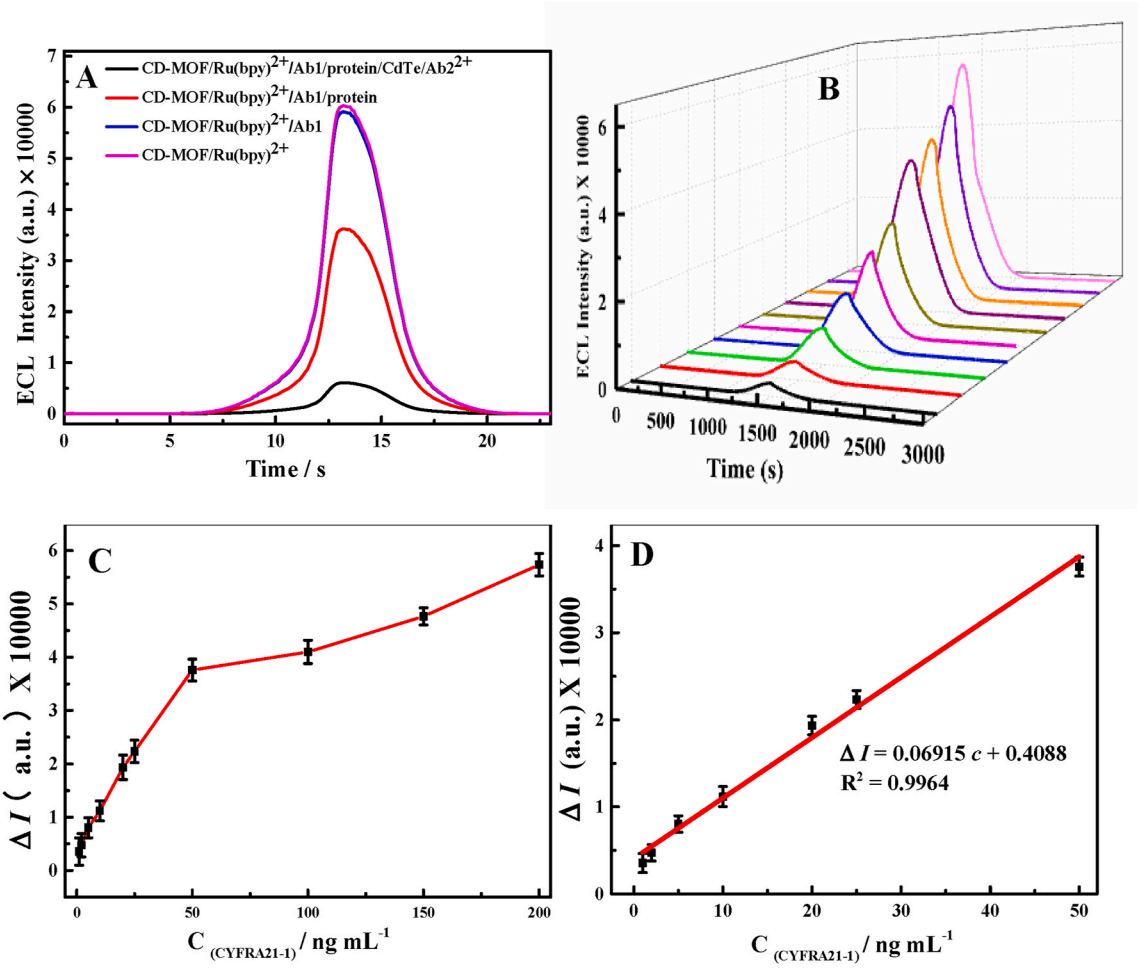

Fig. 3. (A) Cyclic ECL curves of CD-MOF@Ru(bpy)$_3^{2+}$ (pink curve), CD-MOF@Ru(bpy)$_3^{2+}$/Ab1 (blue curve), CD-MOF@Ru(bpy)$_3^{2+}$/Ab1/protein (red curve), and CD-MOF@Ru(bpy)$_3^{2+}$/Ab1/CYFRA21-1/CdTe/Ab2 (black curve) in HCl-Tris buffer solution. (B) The ECL intensity response of the obtained CD-MOF@Ru(bpy)$_3^{2+}$ in 0.1 M Tris-HCl (pH 7.4) containing TPA at different concentrations of CYFRA21-1 from 0.1 to 200 ng mL^{-1}. (C) The line relationship of the ECL intensity and the concentrations of CYFRA21-1 from 0.1 to 200 ng mL^{-1}. The electrolyte was 0.1 M Tris-HCl (pH 7.4) containing TPA. (D) The linear relationships of the ECL intensity and concentrations in 0.1–50 ng mL^{-1}. (For interpretation of the references to colour in this figure legend, the reader is referred to the Web version of this article.)

concentration of the CYFRA21-1 was 0.1–50 ng mL^{-1}, the great line relation could be expressed as $\Delta I = 0.06915c + 0.4088$ ($R^2 = 0.9964$). In this equation, ΔI was $I_0 - I$, I_0 was the ECL intensity from CD-MOF@Ru(bpy)$_3^{2+}$/Ab1/CYFRA21-1 and I was the ECL intensity from CD-MOF@Ru(bpy)$_3^{2+}$/Ab1/CYFRA21-1/CdTe/Ab2. In addition, the detection limit was 0.006 ng mL^{-1}, which was obtained as three times the standard deviation of the blank signal.

Furthermore, the linear range and detection of the proposed ECL biosensor were compared with those of other CYFRA21-1 sensors. The results are shown in Table S1. The biosensor in this work had a low detection limit and satisfactory linear range in comparison with other methods.

3.5. Stability, biocompatibility and selectivity

To investigate the stability of the prepared sensor, CD-MOF@Ru(bpy)$_3^{2+}$ was subjected to 20 continuous cycles with 0.1 M Tris-HCl containing TPA as the co-reagent. As it was shown in Fig. 2B, there was no significant change in the intensity in the resulting ECL curve. In addition, the prepared biosensor was stored at 4 °C and removed for an electrochemical test once a day for 7 days. The results in Fig. S7B displayed that there was no obvious decrease or increase in the response for CYFRA21-1. In brief, these results illustrated that CD-MOF@Ru(bpy)$_3^{2+}$/GCE exhibited high stability and reusability.

Before the biological sample was tested, CD-MOF@Ru(bpy)$_3^{2+}$ was assessed for cytotoxicity using the MTT. The results in Fig. 4A show that the survival rates of A549 lung cancer cells decreased as the volume of CD-MOF@Ru(bpy)$_3^{2+}$ increased. However, more than 85% of the cells survived after being treated with CD-MOF@Ru(bpy)$_3^{2+}$, which proved that CD-MOF@Ru(bpy)$_3^{2+}$ nanocomposites exhibit low toxicity.

To verify the selectivity of the proposed CYFRA21-1 electrochemical biosensor, potential interfering species were also studied, including PSA, CEA, AFP, UA and AA. As shown in Fig. 4B, none of these species caused any observable interference, suggesting acceptable selectivity of the fabricated immunosensor for the determination of CYFRA21-1.

3.6. Application in the real sample analysis

The prepared CD-MOF@Ru(bpy)$_3^{2+}$/GCE sensor was used to detect CYFRA21-1 in a serum using the standard addition method. That is, the real serum sample was diluted 50 times with 0.1 M PBS (pH = 7.4), and then it was measured by ECL after adding to the 5, 10, and 20 ng mL^{-1} CYFRA21-1 protein solution separately. The results were found in Table S2 that the recoveries ranged from 91.60 to 102.2%, suggesting that CD-MOF@Ru(bpy)$_3^{2+}$/GCE has practical utility and could be used for the detection of CYFRA21-1 in blood samples.

In addition, to further test the reliability and feasibility of the developed CD-MOF@Ru(bpy)$_3^{2+}$, it was used to determine the CYFRA21-1 in A549 lung cancer cells which from mouse. That is, certain concentrations of A549 mouse living cells and broken cells were added into the detection system. Then the ECL intensity changes were recorded, and the correlation concentrations were calculated from Fig. 3D. The results were shown in Table 1. It was found that the concentration of the CYFRA21-1 in living cells was between 1.392 and 1.505 ng mL^{-1}, while the concentration of the CYFRA21-1 in broken cells was 10.539–11.283 ng mL^{-1}. In detail, the RSD were 4.0% and 3.5% respectively. Thus, these results showed that this obtained immunosensor was expected to be used for the clinical diagnosis effectively. Besides, in order to determine the reliability of the developed sensor, enzyme-linked immunosorbent assay (ELISA) method had been carried out, and the results were shown in Table 1 and Table S2. It was found that there had the great correlations and coincidences between these two methods.

4. Conclusions

In this work, an enhanced sandwich-type ECL biosensor was constructed for the first time which based on CD-MOF@Ru(bpy)$_3^{2+}$ modified on the GCE. The CD-MOF with large specific surface area and excellent biocompatibility were perfectly combined with the of Ru(bpy)$_3^{2+}$ which had excellent ECL traits. In summary, the sensor showed good sensitivity, high stability and excellent selectivity for the ECL determination of CYFRA21-1. The most important advantage was that the CD-MOF@Ru(bpy)$_3^{2+}$ nanocomposites exhibited low toxicity towards A549 lung cancer cells. This design could be expected as an alternative analytical method to application the ECL biosensors in biological detection.

CRediT authorship contribution statement

Yunfei Wang: Investigation, Formal analysis, Writing - original draft. **Yixiao Li:** Investigation, Visualization. **Xuming Zhuang:** Project administration, Writing - review & editing. **Chunyuan Tian:** Writing - review & editing. **Xiuli Fu:** Supervision. **Feng Luan:** Supervision,

Table 1
Determination for the concentrations of the CYFRA21-1 in A549 cells.

Sample	Time	$C_{CYFRA21-1}$ (ng mL^{-1})	ELISA (ng mL^{-1})	RSD (%)
Living cells	1	1.431	1.426	4.0
	2	1.505	1.497	
	3	1.392	1.403	
Broken cells	4	11.088	11.072	3.5
	5	10.539	10.545	
	6	11.283	11.266	

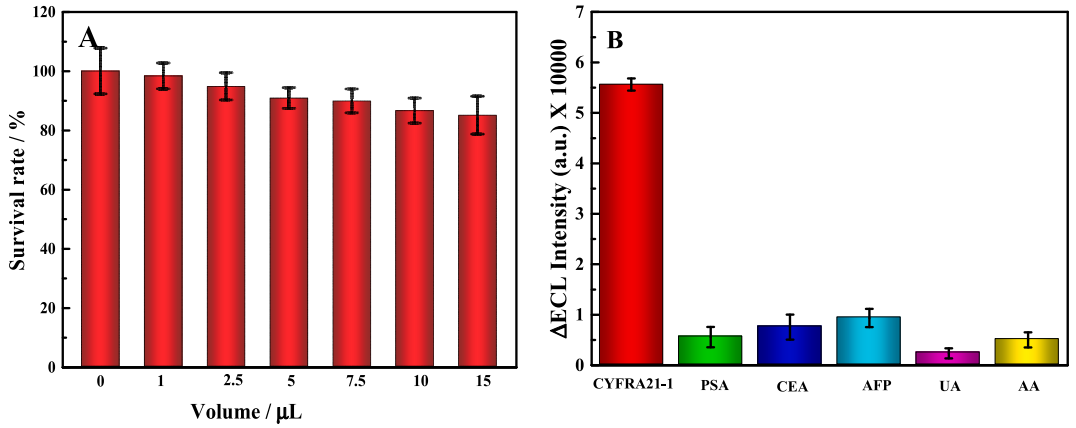

Fig. 4. (A) Survival rate test of A549 cells cultured in a medium with different volumes of CD-MOF@Ru(bpy)$_3^{2+}$. (B) Selectivity of the obtained ECL biosensor was tested in PSA, CEA, AFP, UA, and AA compare to CYFRA21-1 under the same experiment conditions.

Writing - review & editing.

Declaration of competing interest

The authors declare that they have no known competing financial interests or personal relationships that could have appeared to influence the work reported in this paper.

Acknowledgements

This work was financially supported by the National Natural Science Foundation of China (21778047, 21675138).

Appendix A. Supplementary data

Supplementary data to this article can be found online at https://doi.org/10.1016/j.bios.2021.113371.

References

Aizer, A.A., Bi, W.L., Kandola, M.S., Lee, E.Q., Nayak, L., Rinne, M.L., Norden, A.D., Beroukhim, R., Reardon, D.A., Wen, P.Y., 2015. Cancer 121 (24), 4376–4381.
Al-Kutubi, H., Gascon, J., Sudhölter, E., Rassaei, L., 2015. Chemelectrochem 2 (4), 462–474.
Bray, F.I., Ferlay, J., Soerjomataram, I., Siegel, R.L., Torre, L.A., Jemal, A., 2018. CA Cancer J. Clin. 68 (6), 394–424.
Chen, M., Hou, C., Huo, D., Yang, M., Fa, H.B., 2015. Anal. Methods 7 (22), 9466–9473.
Chen, Y.X., Huang, K.J., Niu, K.X., 2018. Biosens. Bioelectron. 99 (15), 612–624.
Fang, Y.H., Li, Y.P., Zhang, M., Cui, B., Hu, Q., Wang, L.S., 2019. Analyst 144 (6), 2186–2194.
Ferrigno, D., Buccheri, G., Giordano, C., 2003. Lung Canc. 41 (3), 311–320.
Han, M.Y., Liu, Q., Yu, J.K., Zheng, S., 2008. J. Clin. Lab. Anal. 22 (2), 131–137.
Hua, Y., Jun, L.I., Zhang, H., Ying, L.V., Shuang, G., 2014. Microporous Mesoporous Mater. 195 (9), 87–91.
Huang, B., Zhou, X., Xue, Z., Wu, G., Du, J., Luo, D., Liu, T., Ru, J., Lu, X., 2013. Talanta 106 (2), 174–180.
Huang, K.J., Liu, X., Xie, W.Z., Yuan, H.X., 2008. Microchim. Acta 162 (1–2), 227–233.
Jia, T.T., Cai, Z.M., Chen, X.M., Lin, Z.J., 2009. Biosens. Bioelectron. 25 (1), 263–267.
Lee, W.Y., Nieman, T.A., 1995. Anal. Chem. 67 (11), 1789–1796.
Li, H.J., Chen, J., Han, S., Niu, W.X., Liu, X.Q., Xu, G.B., 2009. Talanta 79 (2), 165–170.
Luan, F., Wang, Y.F., Zhang, S., Zhuang, X.M., Tian, C.Y., Fu, X.L., Chen, L.X., 2020. Analyst 145 (5), 1943–1949.
Miao, W.J., 2008. Chem. Rev. 108 (7), 2506–2553.
Moussa, Z., Hmadeh, M., Abiad, M.G., Dib, O.H., Patra, D., 2016. Food Chem. 212 (1), 485–494.
Panella, B., Hirscher, M., 2010. Adv. Mater. 17 (5), 538–541.
Peng, J.Y., Wei, L.Y., Liu, Y.X., Zhuge, W.F., Huang, Q., Huang, W., Xiang, G., Zhang, C. Z., 2020. RSC Adv. 10 (60), 36828–36835.
Richter, M.M., 2004. Chem. Rev. 104 (6), 3003–3036.
Rubinstein, I., Bard, A.J., 1981a. ChemInform 103 (3), 512–516.
Rubinstein, I., Bard, A.J., 1981b. ChemInform 103 (17), 5007–5013.
Sun, C., Lu, W., Gao, Y., Li, J., 2009. Anal. Chim. Acta 632 (2), 163–167.
Tian, C.Y., Xu, J.J., Chen, H.Y., 2012. Chem. Commun. 48 (66), 8234–8236.
Torre, L.A., Bray, F., Siegel, R.L., Ferlay, J., Lortet-Tieulent, J., Jemal, A., 2015. CA Cancer J. Clin. 65 (2), 87–108.
Trino, L.D., Albano, L., Granato, D.C., Santana, A.G., Leme, A., 2021. Chem. Mater. 33 (4), 1293–1306.
Waki, K., Yamada, T., Yoshiyama, K., Terazaki, Y., Sakamoto, S., Matsueda, S., Komatsu, N., Sugawara, S., Takamori, S., Itoh, K., 2014. Canc. Sci. 105 (10), 1229–1235.
White, H.S., Bard, A.J., 1982. J. Am. Chem. Soc. 104 (25), 6891–6895.
Xu, Y.T., Xu, L., Qiu, M.T., Wang, J., Zhou, Q., Xu, L., Wang, J., Yin, R., 2015. Sci. Rep. 5 (22), 9444.
Yang, G., Xiao, Z., Tang, C., Deng, Y., Huang, H., He, Z., 2019. Biosens. Bioelectron. 141 (15), 111416.
Yu, S.Q., Zou, G.Z., Wei, Q., 2016. Talanta 156 (15), 11–17.
Zeng, Y., Bao, J., Zhao, Y.A., Huo, D.Q., Chen, M., 2018. Talanta 178 (1), 122–128.
Zhu, Z.Z., Shi, L.F., Feng, H.P., Zhou, S.S., 2015. Bioelectrochemistry 101 (5), 153–158.